Investigating COVID-19 active pharmaceutical ingredients (APIs) degradation using Peroxydisulfate/FeMnOx binary metal oxide/ Ultrasound System

Amin Bagheri [a,b], Akram Fallah [c], Jakub Karczewski [d], Akbar Eslami [a,b], Amir Mohammad Sheikh Asadi [e,f,**], Grzegorz Boczkaj [f,*]

[a] Environmental and Occupational Hazards Control Research Center, Shahid Beheshti University of Medical Sciences, Tehran, Iran
[b] Department of Health, Safety and Environment, School of Public Health and Safety, Shahid Beheshti University of Medical Sciences, Tehran, Iran
[c] Department of Chemical Technologies, Iranian Research Organization for Science and Technology (IROST), Tehran, Iran
[d] Faculty of Applied Physics and Mathematics, Institute of Nanotechnology and Materials Engineering, Gdańsk University of Technology, Narutowicza 11/12 Street, 80-233, Gdańsk, Poland
[e] Chair of Environmental Analytics and Pollutants, Institute IWAR, Technical University of Darmstadt, Franziska-Braun-Straße 7, D-64287, Darmstadt, Germany
[f] Gdańsk University of Technology, Faculty of Civil and Environmental Engineering, Department of Sanitary Engineering, G. Narutowicza 11/12 Str, 80-233, Gdańsk, Poland

ARTICLE INFO

ABSTRACT

Degradation of Favipiravir using a hybrid system of peroxydisulfate, FeMnOx binary metal oxide, and ultrasound irradiation was studied. A novel catalyst was synthesized with deep eutectic solvent (DES). The effects of DES type on catalytic performance was evaluated and the catalysts were characterized using XRD, SEM, BET, XPS, and EDS. DES-based catalysts exhibited higher efficiency due to structure change, surface area enhancement and significantly improved Favipiravir adsorption. The DES-based catalyst exhibited a 30 % increase in surface area and a 20-fold increase in Mn content. Additionally, XRD and XPS analyses suggested the reduction of Fe^{3+} ions, possibly to Fe_3O_4. Optimal operational parameters (pH = 10, catalyst dose = 500 mg/L, and rox = 20) provide removal efficiency of 70.1 % after 3 h. The catalyst showed stable activity after three cycles, indicating reusability. This study presents a promising approach for the sustainable degradation of COVID-19 APIs, with implications for the pharmaceutical industry.

1. Introduction

Active pharmaceutical ingredients (APIs) are one group of contaminants of emerging concern (CECs) that are increasingly being recognized in the environment [1]. During the SARS-CoV-2 pandemic, which caused over 6.3 million deaths worldwide as of July 2022, several antiviral drugs were clinically tested on affected patients with coronavirus disease 2019 (COVID-19). These drugs, including Oseltamivir, RemdeSivir, and Favipiravir, were originally developed against HIV, Ebola, and influenza viruses, respectively

---

In addition, owing to their high adsorption capacity, active sites, abundance, and low toxicity, iron and manganese binary oxides (FeMnOx) have emerged as highly effective catalysts for activating the peroxymonosulfate (PDS) and eliminating organic pollutants [35,36]. Li et al. and Liu et al. proposed that FeMnOx activates peroxymonosulfate by facilitating the cycling of Fe and Mn species during the initiation of radical chain reactions. It is believed that the structural similarity between FeMnOx and O–O bonds allows for the activation of PDS. Furthermore, Fe- and Mn-containing oxides can decompose PDS into $SO_4^{\bullet-}$ [37,38].

The utilization of multi-task solvents such as deep eutectic solvents (DESs) can create favorable conditions during the synthesis processes of metal oxides. The formation of DESs involves the combination of chemicals acting as hydrogen bond donors (HBDs) and hydrogen bond acceptors (HBAs) at specific molar ratios, as initially described by Abbott in Green Chemistry [39]. DESs offer distinct advantages over ionic liquids, including their cost-effectiveness and environmentally friendly nature. These properties have contributed to the increased industrial application of DESs [40]. In the synthesis of nanomaterials, these solvents can serve as non-toxic solvents, reducing agents, precursors, structure-directing agents, templates, and functionalizers [40–42]. For instance, the Choline Chloride (ChCl): Ethylene Glycol (EG) DES has proven effective as a reducing agent in the ultrafast synthesis of manganese oxides, enabling a reaction time as short as one minute [43].

The objective of this study is to employ hybrid SR-AOPs to remove Favipiravir, an antiviral API related to COVID-19, from aqueous solutions. A novel catalyst obtained through DES-assisted synthesis was successfully developed and utilized in the peroxydisulfate/FeMnOx binary metal oxide/ultrasound (PDS/DES-FeMnOx/US) system. The impact of different hydrogen bond donors and choline chloride (ChCl), a well-known and widely used HBA, was systematically assessed to determine their effects on the catalytic performance of the prepared FeMnOx catalyst. Based on our findings, no DES-FeMnOx nanocatalyst has been previously prepared to activate PDS for the removal of Favipiravir from aqueous media. Furthermore, the influence of different HBAs and ChCl on the properties of the final catalyst and its removal behavior requires further investigation and clarification. Therefore, the present work aims to investigate the effects of DESs on the synthesized FeMnOx catalyst and determine the optimal operational conditions for the PDS/DES-FeMnOx/US system.

2. Materials and methods

2.1. Chemical and reagents

The DESs were prepared using two highly pure hydrogen bond donors (HBDs): ethylene glycol (EG, >99 %) and DL-Dithiotheritol (DDT, ≥98 %). Additionally, the hydrogen bond acceptor (HBA) used was choline chloride (ChCl, ≥98 %). These chemicals were obtained from Merck, Germany, except for EG, which was provided by Chempur, Poland.

To synthesize the nanocatalysts, $FeCl_3$ (≥98 %, Merck, Germany) was subjected to dehydration for 2 h at 120 °C under vacuum conditions. $KMnO_4$ (≥99 %, POCH, Poland) was utilized without the need for further purification. To monitor the degradation process, Favipiravir (98 %) was sourced from CHEMAT, Poland, and $N_2S_2O_8$ (PDS, ≥98 %) was acquired from Merck, Germany. Additional chemicals and solvents of analytical grade were used throughout the experiments without undergoing purification.

2.2. DES preparation

To obtain ChCl: EG DES, a mixture of HBA and HBD in a 1:2 M ratio was heated at 80 °C for 1 h under continuous mixing (350 rpm, 06-MSH-PRO-T magnetic stirrer) until a clear solution was obtained. For ChCl: DTT, the temperature and mixing time were maintained at 22 °C and 3 h, respectively.

2.3. Synthesizing DES-FeMnOx binary metal oxides

In a typical procedure, 3.16 g of $KMnO_4$ were dissolved in 400 mL of deionized water by blending for 15 min using a magnetic stirrer at 30 °C. Subsequently, 14.59 g of $FeCl_3$ were dissolved in 90 mL of deionized water and added to the previous solution under vigorous magnetic stirring. After a period of time, the prepared solution was gently introduced to 35 mL of DESs with agitation at 350 rpm, resulting in the formation of a dark brownish-colored slurry. To halt the reaction, approximately 400 mL of deionized water was poured into the beaker. The as-prepared slurry was then filtered using a vacuum pump and washed four times with 1 M H_2SO_4 (≥98 %, Merck). The collected precipitate was subsequently dried at 100 °C for 2 h under a vacuum to obtain the final product. Finally, each product was calcinated at 350 °C for 2 h with a heating rate of 3 °C/min. The products prepared in EG:ChCl and DTT:ChCl DESs were labeled as EG@DES-FeMnOx and DTT@DES-FeMnOx, respectively.

For comparative purposes, the same synthesis procedure was repeated, replacing DES with an equivalent molar amount of ethylene glycol (EG) as the reducing agent. This was done to assess the influence of DES-assisted synthesis on the properties of the catalyst. The resulting product was named EG-FeMnOx.

2.4. Catalyst characterization

The morphology and elemental composition of the materials were analyzed using the FEI Quanta FEG 250 scanning electron microscope (SEM) equipped with an ET secondary electron detector and an Apollo X SDD energy-dispersive spectrometer (EDS). The acceleration voltage was maintained at 10 kV for imaging and 20 kV for EDS measurements. The EDS data were analyzed using the EDAX Genesis APEX 2i software. The phase composition of the samples was analyzed using a Bruker D2 Phaser 2nd generation X-ray

diffractometer. CuKα radiation and a LynxEye XE-T detector were employed for analysis at room temperature. Nitrogen adsorption-desorption isotherms were measured using a surface area analyzer, specifically the NOVAtouch™ 2 instrument from Quantachrome Instruments, at a temperature of 77 K. Prior to the measurements, the samples were degassed under vacuum at 120 °C for 4 h. The specific surface area was calculated using the Brunauer-Emmett-Teller (BET) linear equation within the approximate relative pressure range of 0.1–0.3. The correlation coefficient of the linear regression was determined to be not less than 0.999. The XPS analysis was performed using a Thermo Scientific K-Alpha X-ray Photoelectron Spectrometer (XPS) instrument, equipped with a high-resolution XPS detector for accurate elemental analysis.

2.5. Degradation experiments

In this study, the removal of Favipiravir was performed using heterogeneous SR-AOPs under US irradiation. The experimental setup consisted of Hielscher UP400St ultrasonic probe laboratory-scale installations, which included a 700-mL acid-proof steel reactor equipped with a tap water-cooling cycle system. For the investigation of sonocavitation, a sonotrode (S24d7) operating at a fixed frequency of 24 kHz and delivering an acoustic power output of 164 W was utilized. Fig. 1 illustrates the configuration of the sonocavitation reactor.

In a typical degradation process, 10 mg of Favipiravir was dissolved in 500 mL of deionized water for 1 h (resulting in a 20-ppm solution). To adjust the pH, NaOH (1 N) and H2SO4 (1 N) were employed. Subsequently, a specified amount of catalysts (100, 500, and 800 mg/L) was introduced into the solution. Equilibrium of adsorption and desorption was obtained within a period of 30 min, which was consistent across all experimental setups. Following that, the sonotrode was positioned at the center of the reactor, and US irradiation was initiated. Furthermore, the PDS concentration was regulated by adding 0.8 mL of stock PDS solutions every 15 min for 1 h, aiming to achieve different oxidant to dioxane ratios (approximately 5, 20, and 50).

The addition of such a procedure resulted in the prohibition of self-scavenging of PDS. This approach has already been demonstrated to be effective in our previous study [44]. Subsequently, a 1 mL aliquot of the processed sample was promptly injected into the HPLC system (Hitachi LaChrom Elite® HPLC) equipped with a C18 column (4.5×150 mm, Agilent, USA) and a UV detector (Merck-Hitachi UV–Vis L-7420). For the analysis of Favipiravir, a mobile phase consisting of 90:10 v/v of 0.5 mM H_2SO_4 (pH = 3) and acetonitrile was employed, with a flow rate of 0.8 mL/min. The monitored wavelength for Favipiravir was set at 320 nm. The limit of detection (LOD) and limit of quantification (LOQ) for Favipiravir were determined to be 0.2 and 0.4 ppm, respectively.

For the recycling experiments, following the degradation process, the reaction media was allowed to settle for 1 h. The prepared catalysts were then easily collected using a magnet and treated with 1 M H_2SO_4. Subsequently, they were filtered and dried for 2 h under vacuum conditions at 100 °C. These dried catalysts were employed for three consecutive cycles. To gather information on the leaching of Fe and Mn from the catalysts, three systems - US/catalyst, PDS/catalyst, and US/PDS/catalyst - were utilized. Additionally, a blank sample was included for the leaching experiments. The collected samples underwent analysis using ICP-OES in accordance with ISO 11885:2009 to detect and quantify the released Fe and Mn ions.

1. Coolant inlet
2. Coolant outlet
3. Reaction media
4. Anechoic chamber
5. Ultrasonic generator
6. Sonotrode
7. Power source

Fig. 1. Experimental setup for the SR-AOP-based degradation of Favipiravir.

3. Results and discussion

3.1. Catalyst structure assessment

The morphologies of the synthesized EG-FeMnOx and EG@DES-FeMnOx were investigated through scanning electron microscopy (SEM), as shown in Fig. 2. It is evident from the images that there was significant agglomeration observed in the case of EG-FeMnOx. In contrast, the particles of EG@DES-FeMnOx exhibited a modified-ordered surface, which facilitated improved interconnection and activation of the PDS as an oxidant. The SEM morphology images further confirm that the addition of ChCl as an HBA along with EG as an HBD enhanced the dispersibility of FeMnOx particles, resulting in reduced agglomeration in the final product. Thus, the use of EG: ChCl DES proved to be a valuable reagent, effectively addressing the challenge of self-agglomeration encountered with FeMnOx binary oxide particles.

The elemental content of two selected samples, EG-FeMnOx and EG@DES-FeMnOx, was analyzed using EDS analysis. The results are depicted in Fig. 3. As shown in Table 1, the weight ratios of Fe to Mn in EG-FeMnOx and DES-based FeMnOx are 66.15:0.14 and 74.39:2.89, respectively. This indicates that the Fe to Mn ratio in EG-FeMnOx is approximately 472.5, while in EG@DES-FeMnOx, it is 25.74. Consequently, the synthesis of FeMnOx in DES (EG: ChCl) led to a 20-fold increase in Mn weight content, corresponding to an atomic ratio of Fe–Mn (48.92/1.93). It appears that DES acted as a template, maintaining the metal oxides in a more suitable ratio. In other words, the presence of DES facilitated the reduction of Mn^{+7} and Fe^{+3}, a finding further supported by XRD analysis. Based on degradation experiments, it can be inferred that the higher Mn content in EG@DES-FeMnOx, which possesses a higher reduction potential, contributed significantly to the enhanced AOP-based degradation of Favipiravir.

Fig. 4 illustrates the nitrogen adsorption-desorption isotherms and the specific surface area of two catalysts synthesized after undergoing 2 h of calcination at 350 °C. The physisorption isotherms of this catalyst exhibit a type V isotherm according to the IUPAC classification, accompanied by distinct hysteresis loops, which are indicative of the presence of mesopores ranging from 2 to 50 nm in

(a)

(b)

Fig. 2. SEM analysis of (a) EG-FeMnOx and (b) EG@DES-FeMnOx.

(a)

(b)

Fig. 3. EDS analysis of (a) EG-FeMnOx and (b) EG@DES-FeMnOx.

width. The presence and shape of the hysteresis provide evidence of mesoporosity within the samples. This characteristic is advantageous as it facilitates efficient mass transport within the catalyst by offering favorable diffusion properties. Specifically, the EG-FeMnOx catalyst possesses slit-shaped pores, while the EG@DES-FeMnOx catalyst exhibits cylindrical pores.

The adsorptive behavior of the synthesized binary systems is significantly influenced by their specific surface areas, as demonstrated in Fig. 4. The total specific surface area of EG-FeMnOx is measured at 26.9 m^2/g, whereas EG@DES-FeMnOx exhibits a higher value of 38.3 m^2/g. The utilization of the HBD: HBA system as a solvent leads to an enlargement of pore size from slit to cylindrical

Table 1
Elemental parameters of EG-FeMnOx and EG@DES-FeMnOx calculated from the EDS analysis.

Elements	EG-FeMnO$_x$		EG@DES-FeMnO$_x$	
	Weight (%)	Atomic (%)	Weight (%)	Atomic (%)
O	32.22	62.20	20.47	46.99
S	0.21	0.20	0.69	0.79
Cl	0.67	0.58	0.83	0.86
Cr	0.61	0.36	0.71	0.50
Mn	0.14	0.08	2.89	1.93
Fe	66.15	36.58	74.39	48.92
Total	100	100	100	100

Fig. 4. Brunauer-Emmett-Teller (BET): Specific surface area of a) EG@DES-FeMnOx and b) EG-FeMnOx and adsorption/desorption isotherm of c) EG@DES-FeMnOx and d) EG-FeMnOx.

geometry, accompanied by an increase in surface area. It is worth noting that the mesoporous structure of the samples likely contributes to greater accessibility of active sites for the activation of PDS and adsorption of Favipiravir [45,46].

The compositions of the selected samples were confirmed through the X-ray diffraction (XRD) analysis. Fig. 5 illustrates the XRD patterns of hematite (Fe_2O_3) and magnetite ($FeFe_2O_4$) in both diagrams, displaying similar diffraction peaks while exhibiting varying intensities. It is evident that the diffraction peaks corresponding to hematite in the EG@DES-FeMnOx sample were noticeably reduced compared to those in the EG-FeMnOx sample. This transformation can be attributed to the presence of DES, which facilitated the reduction of Fe^{+3}. Moreover, DES-containing catalysts exhibited broader diffraction peaks, indicating the presence of smaller grain sizes. These findings were consistent with SEM results. Furthermore, the sharp and intense diffraction peaks observed in both samples indicated their high crystallinity, which was a consequence of the calcination procedure. In XRD analysis, the distinctive patterns of hematite and magnetite generally allow for clear differentiation from those of manganese oxides. However, when the concentration of manganese oxides is notably lower compared to these iron compounds, as is the case in our study, it is plausible for the XRD patterns of manganese oxides to be partially concealed by the presence of Fe_2O_3 or Fe_3O_4. To ensure accurate identification and distinction of manganese oxides, supplementary techniques such as SEM-EDS and XPS were employed alongside the XRD data. Notably, EDS analysis confirmed the presence of manganese, albeit in a limited quantity. Additionally, XPS analysis identified Mn 2p, albeit at a low concentration, aligning with our initial hypothesis.

Fig. 5. XRD patterns of (a) EG-FeMnOx and (b) EG@DES-FeMnOx

The high-resolution Fe 2p spectra for the synthesized samples in both ethylene glycol and DES solvents are illustrated in Fig. 6.
Fig. 6 suggests that these spectra can be deconvoluted into five distinct peaks, representing Fe^{2+} 2p3/2, Fe^{3+} 2p3/2, Fe^{2+} 2p1/2, Fe^{3+} 2p1/2, and a satellite peak [1,2] [47,48]. The presence of iron elements in both the 2+ and 3+ states indicates the coexistence of hematite (Fe^{3+}) and magnetite (Fe^{2+} + Fe^{3+}) forms in both samples. However, to determine the atomic percentages of these states, one must measure the area beneath the peaks.

As can be seen in Table 2, the data reveals that in the sample synthesized using ethylene glycol as the solvent, the atomic percentages of Fe^{2+} and Fe^{3+} were 31.24 % and 68.76 %, respectively. Conversely, in the sample synthesized with DES as the solvent, these percentages shifted to 52.62 % for Fe^{2+} and 47.38 % for Fe^{3+}. This higher proportion of Fe^{2+} in the DES-synthesized sample highlights the predominance of the magnetite phase in this particular sample, a result that is consistent with findings obtained through other characterization methods.

3.2. Degradation process assessment

Ultrasonic radiation has the potential to induce sonocavitation within a water-based medium, resulting in the formation of highly intense bubbles. The subsequent collapse of these bubbles leads to a significant rise in local temperature and pressure, ultimately leading to the generation of hydroxyl radicals (•OH). At high temperatures, the weak bond dissociation energy of H_2O_2 prevents •OH

Fig. 6. XPS high-resolution spectra of Fe 2p for synthesized samples in ethylene glycol and DES solvents.

8

Table 2

The obtained data from deconvolution of Fe 2p spectra.

Solvent	States	Peak position (eV)	Peak area (CPS.eV)	%At.
Ethylene glycol	Fe^{2+} $2p_{3/2}$	709.4	54957.7	27.39
	Fe^{3+} $2p_{3/2}$	710.9	84677.3	42.20
	Fe^{2+} $2p_{1/2}$	722.9	7720.4	3.85
	Fe^{3+} $2p_{1/2}$	723.2	53282.8	26.56
DES	Fe^{2+} $2p_{3/2}$	709.1	55448.2	33.10
	Fe^{3+} $2p_{3/2}$	711.2	63398.6	37.84
	Fe^{2+} $2p_{1/2}$	723.8	32700.8	19.52
	Fe^{3+} $2p_{1/2}$	725.3	15985.5	9.54

radicals from recombining. This leads to ●OH radicals dispersing into the main solution, resulting in a notably high concentration, approximately 10^{-2} M, at the bubble surface. These hydroxyl radicals play a crucial role in decomposing organic pollutants in AOPs [49]. Additionally, the utilization of US waves generates acoustic flow and turbulence, thereby mitigating the challenges associated with mass transfer within the medium [28].

Cavitation bubbles also can activate sulfate-based AOPs, whereby PDS produces $SO_4^{\bullet-}$ [50]. As depicted in Fig. 7, the sole PDS process exhibited no discernible impact on the degradation of Favipiravir, indicating that PDS necessitates activation to effectively decompose this pharmaceutical compound. Moreover, the implementation of ultrasonic irradiation resulted in a 34.3 % reduction in pollutant concentration after 3 h. The incorporation of PDS into the aforementioned system elevated its efficacy, leading to a 42.2 % reduction during the same time frame. However, further refinement of this approach was imperative to achieve satisfactory results. In light of the advantages demonstrated by catalytic AOPs in pharmaceutical pollutant degradation, non-toxic and cost-effective FeMn binary oxides were utilized to activate PDS and enhance degradation efficiency.

For the synthesis of FeMn binary oxides, two types of DESs were prepared, namely ChCl: EG and CHCl: DTT, with a molar ratio of 1:2, serving as the reducing agents. Subsequent degradation experiments were conducted to identify the most promising catalyst among EG@DES and DTT@DES-based nanoparticles.

In Fig. 8, the impact of each synthesized catalyst on various removal processes was investigated. When the sole catalyst process was responsible for removing Favipiravir, it was observed that the EG@DES-based catalyst adsorbed a significantly higher amount of the target pollutant (20.2 %) compared to the DTT@DES-based catalyst (5.89 %). The introduction of ultrasound in conjunction with the catalyst slightly enhanced the removal efficiency in both groups. However, the utilization of the catalyst in combination with the PDS system yielded distinct behaviors for the synthesized catalysts. The synergistic application of US, PDS, and the catalyst led to a significant improvement in the degradation process, particularly when the EG@DES-based catalyst was employed (50.3 %). Consequently, the EG@DES-FeMnOx catalyst was selected for subsequent optimization studies.

Research findings suggest that the US/PDS/catalyst system shows promise for the degradation of Favipiravir, with outcomes indicating an increase in reactive oxygen species (ROS) due to PDS activation through US irradiation (see Fig. 7). Typically, a higher concentration of PDS leads to enhanced generation of radicals like $SO4^{\bullet-}$, thereby improving pollutant removal rates. However, it is important to note that once a certain concentration threshold is reached, the decomposition begins to decline due to the scavenging effect of PDS [28]. Since this phenomenon has been observed in various studies, it becomes crucial to identify the optimal PDS concentration at which the scavenging effect limits the overall effectiveness of the process.

To determine the optimal PDS concentration, 3 M ratios of PDS to Favipiravir were selected (approx. 5, 20, and 50, as shown in Fig. 9). To mitigate the disadvantages associated with the scavenging phenomenon, a stepwise injection of oxidants was employed to counteract the adverse effects [44]. Therefore, a plan was devised to inject PDS into the reaction media every 15 min, allowing for the

Fig. 7. Removal efficiency of PDS, US, and their coupled system for decomposing of Favipiravir.

Fig. 8. Comparing the removal activity of synthesized catalysts in different processes for degradation of Favipiravir (20 ppm) under the following experimental conditions: Dose of catalysts = 500 mg/L, T = 60 min, and rox = 20.

Fig. 9. Effect of PDS concentration on Favipiravir decomposition under US irradiation. Conditions: dose of catalysts = 500 mg/L, T = 60 min, molar ratio of the PDS to Favipiravir (rox: = 5:1 (PDS = [0.63 mM]), 20:1 (PDS = [2.5 mM]) and 50:1 (PDS = [6.3 mM]).

Table 3
pH effect on various removal processes.

No	pH	US	Catalyst	r_{ox}	k	Removal (3h)
–	–	100 %	500 mg/L	20	1/min	%
1	NC[1]	*	*	–	NP[2]	NP
2	NC	*	–	*	0.003	42.23
3	NC	–	*	*	NP	NP
4	NC	*	*	*	0.0035	47.33
5	3	*	*	–	NP	NP
6	3	*	–	*	0.0033	44.76
7	3	–	*	*	NM[3]	NM
8	3	*	*	*	0.0049	58.63
9	10	*	*	–	0.0035	47.51
10	10	*	–	*	0.004	52.27
11	10	–	*	*	0.0012	30.24
12	10	*	*	*	0.0065	70.07

[1] NC = not corrected, pH ≈ 5.
[2] NP = not performed.
[3] NM = not measurable.

measurement of the final approximate ratio of oxidant to Favipiravir within 1 h.

The removal efficiency significantly increased from less than 5 % to approximately 20 % by raising the rox from 5 to 20. Although there was an observed increase as rox reached 50, it was not deemed statistically significant, potentially attributable to the initiation of the scavenging effect. Consequently, a rox value of 20 was considered cost-effective and chosen as the optimized point.

The importance of pH in AOPs is widely recognized. Hence, three distinct pH conditions were taken into account: basic (pH = 10), acidic (pH = 3), and non-modified (pH ≈ 5) conditions.

A comprehensive analysis of the data presented in Table 3 highlights the remarkable removal efficiency achieved when employing the US/PDS/catalyst system at a pH of 10, resulting in a removal rate of 70.07 %. Intriguingly, investigations conducted at a pH of 3 demonstrate superior removal after 3 h of degradation compared to a pH of 5. These findings underscore the potential of persulfate activation under both acidic and basic conditions in water depollution processes, owing to their distinct properties. It is important to note that the degradation kinetics are enhanced in alkaline conditions.

In environments characterized by low pH, specifically acidic conditions with a pH of 3, persulfate activation occurs through Fenton-like reactions facilitated by iron, leading to the generation of sulfate radicals. Activation of persulfate at acidic pH levels exhibits oxidizing capabilities similar to hydroxyl radicals ($\bullet$OH). Conversely, as the pH of the environment increases (reaching pH 10), persulfate activation intensifies, placing a greater emphasis on kinetic enhancement. The presence of hydroxyl radicals not only directly contributes to the efficiency of degradation but also stimulates the generation of persulfate radicals, thereby amplifying the overall removal efficiency. Additionally, considering the pKa value of Favipiravir, which is 5.1, it predominantly exists as a protonated molecule above this pH. On the contrary, the acidification of the as-synthesized catalyst creates a surface with a more positive charge, facilitating interaction with the ionic form of Favipiravir and leading to an improvement in removal efficiency [51,52].

The degradation kinetics of Favipiravir were investigated using the Langmuir-Hinshelwood model, which is expressed by Equation (3):

$$\ln(C_i/C_f) = -kt \qquad\qquad 3$$

Within this equation, the term $\ln(C_i/C_f)$ denotes the natural logarithm of the ratio between the initial concentration (C_i) and the final concentration (C_f) of Favipiravir at a specific time (t) measured in minutes. The negative sign associated with the equation signifies the decrease in concentration over time. The rate constant (k) plays a crucial role in determining the reaction rate for the degradation process, indicating the occurrence of pseudo first-order reaction kinetics. In the case of the US/PDS/catalyst system, the pseudo-first order rate constant values (k) were found to be 0.0035, 0.0049, and 0.0065 min^{-1} for the not-modified, acidic, and basic conditions, respectively, which align with the removal efficiency of each condition. Furthermore, based on Equation (3), the US/PDS/catalyst system at pH 10 indicates a synergistic effect value (SEV) of 1.13, representing the synergistic performance of the three processes in the hybrid system.

$$\text{Synergistic Effect Value(SEV)} = \frac{\text{Favipiravir Removal (US/PDS/catayst)}}{\text{Favipiravir Removal(US)} + \text{Favipiravir Removal(PDS)} + \text{Favipiravir Removal (catalyst)}} \qquad\qquad 4$$

The synergistic effect of hybrid processes was assessed through the investigation of Favipiravir removal in the studied processes. No further experiments were conducted to reveal the synergistic effects under not-modified and acidic conditions due to their lower effectiveness.

To optimize the catalyst dosage, concentrations of 100, 500, and 800 mg/L were tested (Fig. 10). This range was evaluated considering that the use of 1000 mg/L of catalyst would be impractical for industrial applications due to the substantial amount of

Fig. 10. Effect of different doses of catalysts for decomposition of Favipiravir under the following conditions: Dose of catalysts = 100, 500, and 800 mg/L, T = 180 min, rox 20, and concentration of Favipiravir = 20 ppm.
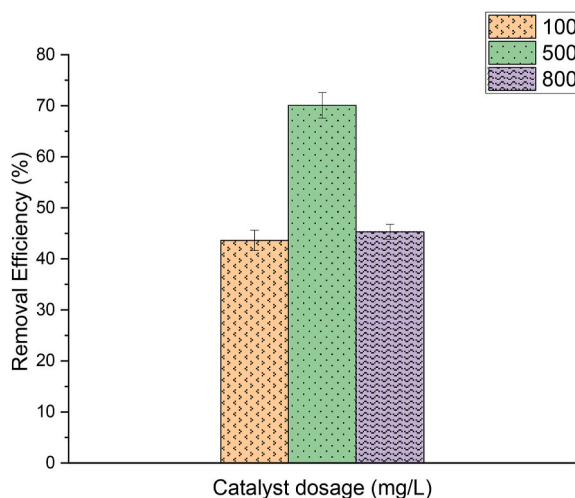
catalyst required per day, even for a small wastewater treatment plant. Doses below 100 mg/L were also found to be ineffective; hence, this range was chosen.

The results clearly demonstrate that the removal efficiencies at the upper and lower borders of the selected range are significantly lower than those at the midpoint. Therefore, the optimal condition for the catalyst dosage is 500 mg/L, which achieves approximately 70 % effectiveness after 3 h. The catalyst's magnetic properties facilitate effective separation and reuse after treatment. Consequently, the optimum conditions for Favipiravir degradation in the US/PDS/catalyst system are as follows: pH = 10, catalyst dosage = 500 mg/L, and rox = 20. Several studies were conducted to investigate the effectiveness of different catalysts and ultrasonic irradiation in the removal of complex organic materials. For instance, a study by Jamalluddin and Zuhairi Abdullah focused on the removal of Reactive Blue 4 dye using a combination of a 0.4 Fe^{3+}/TiO_2 catalyst, aeration, and ultrasonic irradiation. The results showed a remarkable removal efficiency of 96 %, with an optimal catalyst concentration of 1.5 g/L resulting in a degradation rate of 90 % under sonocatalytic conditions. Another study by Muruganandham et al. aimed to examine the impact of ultrasonic irradiation at a frequency of 35 kHz on the catalytic activity and stability of goethite powder (α-FeOOH) in the presence of H_2O_2. They investigated the role of goethite in the decomposition process and analyzed the effect of catalyst loading (2.5−15 g/L) on the decolorization of Direct Orange 39 dye. The optimal quantity of catalyst to be added was found to depend on various experimental factors and the nature of the organic pollutants being treated. It was also noted that other studies suggested a recommended dosage of approximately 500 mg/L or higher.

3.3. Role of DES assisted catalyst synthesis

To investigate the impact of sole ethylene glycol on catalyst behavior in the absence of DES-based media for synthesis, the EG-FeMnOx catalyst was utilized in the degradation process under optimized conditions. After a duration of 3 h, only a 41 % removal of Favipiravir was observed. Although the successful synthesis of EG-FeMnOx catalyst is apparent, the catalysts synthesized in the presence of DES exhibited greater effectiveness during the degradation process.

Catalyst characterization revealed that EG-FeMnOx exhibited a higher hematite phase compared to the DES-based catalyst, indicating a greater presence of Fe_2O_3 in the synthesized catalyst. Conversely, the DES-based catalyst exhibited a higher Fe_3O_4 structure, suggesting reduced reduction in the absence of DES. Additionally, EDS analysis not only corroborated the XRD results but also indicated that the use of EG resulted in insignificant Mn reduction.

As previously mentioned, DES had the ability to enhance the surface area and modify the morphology of the synthesized catalyst. These advancements led to an improvement in Favipiravir adsorption, as the results indicated negligible adsorption (<1 %) when utilizing EG-FeMnOx, whereas the DES-based catalyst exhibited approximately 20 % removal under the same conditions (pH = 10, catalyst dosage = 500 mg/L, and initial concentration = 20 mg/L).

3.4. Recycling, reusability, and stability of EG & DES-FeMnOx

Transition metal ion leaching is a major concern in industries when utilizing metal-based catalysts, as it can result in secondary pollution. Furthermore, the recyclability of catalysts is predominantly evaluated based on their durability and efficiency in oxidizing pollutants. Consequently, we conducted experiments to investigate the leaching of Fe and Mn ions through the EG@DES-FeMnOx/PS/US (No. 1), EG@DES-FeMnOx/PDS (No. 2), and EG@DES-FeMnOx/US (No. 3) systems, aiming to assess the catalyst's reusability (as shown in Table 4).

As shown in Table 4, the concentrations of Fe and Mn were analyzed in four samples. The leaching percentages of Mn ranged from 1 to 2.6 % across the three studied systems (Table 4, No. 1–3). In contrast, the leaching of Fe ions in the three studied systems (Table 4, No. 1–3) varied from trace amounts (<0.1 mg/L) to a significant value (20.6 mg/L). When US and PDS were used individually, the release of Fe was significant. However, when the treatment process involved EG@DES-FeMnOx/US/PDS, the release of both Fe and Mn ions into the reaction media was insignificant. Furthermore, in this experiment, a higher percentage of Fe ions leached compared to Mn ions, which could be attributed to the higher weight percentage of Fe than Mn.

Furthermore, to assess the catalyst efficiency, three recycling tests were conducted for Favipiravir decomposition using EG@DES-FeMnOx/PS/US. Typically, the catalyst was separated after each cycle using a magnet, washed with 1 M sulfuric acid for an hour, collected through vacuum filtration, and dried for subsequent cycles. Initially, deionized water was used in the recycling process; however, preliminary results indicated that the catalyst's activity was not fully maintained, and its efficiency significantly decreased after the first cycle. To address this issue, acid treatment was proposed as a promising solution. As illustrated in Fig. 11, after three cycles, a reasonable level of degradation was still achieved.

3.5. Proposed mechanisms for the removal of favipiravir

The combination of persulfate (PDS), FeMnOx catalyst, and ultrasonic waves (US) offers a promising approach for degrading Favipiravir. The adsorption of Favipiravir on the surface of FeMnOx catalysts enhances the degradation process by increasing contact and facilitating the proximity of generated radicals to the adsorbed compound. Consequently, the likelihood of radical attack and subsequent degradation is significantly enhanced.

Ultrasonic waves generate cavitation bubbles in the solution, leading to the formation of highly reactive hydroxyl radicals ($\bullet OH$) that play a crucial role in oxidizing and degrading organic compounds. Moreover, the addition of PDS acts as a radical initiator, activating sulfate and sulfite radicals ($SO_5^{\bullet-}$, $S_2O_8^{\bullet-}$, and $SO_4^{\bullet-}$) to further enhance the oxidative capacity of the system.

The proposed degradation mechanism in the PDS/DES-FeMnOx/US system involves a series of intricate reactions. Ultrasonic waves

Table 4
Fe and Mn leaching in different treatment systems.

No	properties		
	Treatment systems	Leaching detected ions	Ion amounts (mg/L)
1	catalyst/US/PDS	Fe	<0.1
		Mn	1.0
2	catalyst/PDS	Fe	10.6
		Mn	1.1
3	catalyst/US	Fe	20.6
		Mn	2.6
4	Blank	Fe	<0.1
		Mn	<0.1

Fig. 11. Reusability of EG-DES-FeMnOx in the catalyst/US/PDS system for decomposition of Favipiravir under the following condition: dose of catalysts = 500 mg/L, T = 180 min, rox 20, pH = 10 and concentration of Favipiravir = 20 ppm.

(US) generate hydrogen ions, hydroxyl radicals, and sulfate radicals from water and persulfate ions. Fe^{+2} ions react with hydroxyl radicals, forming Fe^{+3} ions and hydroxide ions. Similarly, Mn^{+2} ions react with persulfate ions, resulting in Mn^{+3} ions and sulfate radicals. Additionally, Mn^{+2} ions can be oxidized by hydroxyl radicals to produce Mn^{+3} ions and hydroxide ions. Sulfate radicals can react with persulfate ions or with each other, generating persulfate anions and molecular oxygen. Furthermore, sulfite radicals, formed from reactions with water or hydroxyl sulfate ions, can undergo reactions with each other or with sulfate radicals, resulting in the formation of persulfate anions and molecular oxygen (Eqs. (5)–(22)). Collectively, these reactive species contribute to the degradation process of Favipiravir.

$$US + H_2O \rightarrow H^+ + HO^\bullet \tag{5}$$

$$US + S_2O_8^{2-} \rightarrow 2SO_4^{\bullet-} \tag{6}$$

$$Fe^{+2} + S_2O_8^{2-} \rightarrow Fe^{+3} + SO_4^{\bullet-} + SO_4^{2-} \tag{7}$$

$$Fe^{+2} + SO_4^{\bullet-} \rightarrow Fe^{+3} + SO_4^{2-} \tag{8}$$

$$Fe^{+2} + HO^\bullet \rightarrow Fe^{+3} + OH^- \tag{9}$$

$$Fe^{+3} + S_2O_8^{2-} \rightarrow Fe^{+2} + S_2O_8^{\bullet-} \tag{10}$$

$$Mn^{+2} + S_2O_8^{2-} \rightarrow Mn^{+3} + SO_4^{\bullet-} + SO_4^{2-} \tag{11}$$

$$Mn^{+3} + S_2O_8^{2-} \rightarrow Mn^{+2} + S_2O_8^{\bullet-} \tag{12}$$

$$Mn^{+2} + HO^\bullet \rightarrow Mn^{+3} + OH^- \tag{13}$$

$$SO_4^{\bullet-} + S_2O_8^{2-} \rightarrow SO_4^{2-} + S_2O_8^{\bullet-} \tag{14}$$

$$SO_4^{\bullet-} + SO_4^{\bullet-} \rightarrow S_2O_8^{2-} \tag{15}$$

$$SO_4^{\bullet-} + H_2O \rightarrow SO_4^{2-} + HO^\bullet + H^+ \tag{16}$$

$$SO_4^{\bullet-} + HO^\bullet \rightarrow HSO_5^- \tag{17}$$

$$S_2O_8^{\bullet-} + Fe^{+3} + 2H_2O \rightarrow Fe^{+2} + 2HSO_5^- + 2H^+ \qquad\qquad 18$$

$$S_2O_8^{\bullet-} + Mn^{+3} + 2H_2O \rightarrow Mn^{+2} + 2HSO_5^- + 2H^+ \qquad\qquad 19$$

$$SO_4^{\bullet-} + HSO_5^- \rightarrow SO_5^{\bullet-} + SO_4^{2-} + H^+ \qquad\qquad 20$$

$$SO_5^{\bullet-} + SO_5^{\bullet-} \rightarrow S_2O_8^{2-} + O_2 \qquad\qquad 21$$

$$SO_5^{\bullet-} + SO_5^{\bullet-} \rightarrow 2SO_4^{\bullet-} + O_2 \qquad\qquad 22$$

4. Conclusions

For the first time, this study presents a comprehensive investigation into the removal of Favipiravir, a crucial active pharmaceutical ingredient for COVID-19 treatment. The novelty lies in the development of a hybrid system that combines peroxydisulfate, FeMnOx catalyst, and ultrasound irradiation to degrade Favipiravir. A novel catalyst was synthesized using the ethylene glycol: choline chloride deep eutectic solvent (EG@DES), leading to significant advancements in the reduction of Fe and Mn ions compared to conventional EG-based reaction media. Furthermore, the catalysts based on EG@DES exhibited a 1.12-fold increase in surface area, contributing to improved removal efficiency during the degradation process. Some degradation mechanisms were introduced in this study; however, further investigations are required to unravel the underlying mechanisms driving the degradation process. The optimized hybrid system demonstrated a notable removal efficiency of 70.07 % after a 3-h treatment under specific conditions (pH = 10, catalyst dose of 500 mg/L, and rox = 20). Comparisons with previous studies highlight the potential of this hybrid system in degrading Favipiravir. Future research can focus on evaluating its scalability. This study introduces new concepts and innovations in the field of pharmaceutical degradation, provides valuable insights into the hybrid system's performance, and emphasizes its potential for addressing environmental challenges associated with the removal of active pharmaceutical ingredients.

Author contribution statements

We respectfully claim that in the present project, Prof. Boczkaj, and Mr. Sheikh Asadi conceived the presented idea. Mr. Sheikh Asadi and Prof. Amin Bagheri carried out the experiments and developed the methods, and Dr. Fallah conducted the synthesis procedures. Dr. Karczewski accomplished the characterization of the synthesized products of the project. Prof. Bagheri, Prof. Eslami, and Prof. Boczkaj supervised the findings and implementation of this work. Mr. Sheikh Asadi wrote the paper with input from all authors.

Declaration of competing interest

The authors declare that they have no known competing financial interests or personal relationships that could have appeared to influence the work reported in this paper.

Data availability

Data will be made available on request.

Acknowledgments

References

[1] M.A. Chia, A.S. Lorenzi, I. Ameh, S. Dauda, M.K. Cordeiro-Araújo, J.T. Agee, et al., Susceptibility of phytoplankton to the increasing presence of active pharmaceutical ingredients (APIs) in the aquatic environment: a review, Aquatic Toxicology 234 (2021), 105809.

[2] K. Kuroda, C. Li, K. Dhangar, M. Kumar, Predicted occurrence, ecotoxicological risk and environmentally acquired resistance of antiviral drugs associated with COVID-19 in environmental waters, Science of The Total Environment 776 (2021), 145740.

[3] W.H. Organization, WHO coronavirus (COVID-19), Dashboard, https://covid19.who.int/, July 2022.

[4] M.N. Hasan, M.S. Salman, M.M. Hasan, K.T. Kubra, M.C. Sheikh, A.I. Rehan, et al., Assessing sustainable Lutetium (III) ions adsorption and recovery using novel composite hybrid nanomaterials, Journal of Molecular Structure 1276 (2023), 134795.

[5] A. Islam, S.H. Teo, Y.H. Taufiq-Yap, C.H. Ng, D.-V.N. Vo, M.L. Ibrahim, et al., Step towards the sustainable toxic dyes removal and recycling from aqueous solution-A comprehensive review, Resources, Conservation and Recycling 175 (2021), 105849.

[6] M. Kumar, K. Kuroda, K. Dhangar, P. Mazumder, C. Sonne, J. Rinklebe, et al., Potential emergence of antiviral-resistant pandemic viruses via environmental drug exposure of animal reservoirs, Environmental Science & Technology. 54 (14) (2020) 8503–8505.

[7] M.R. Awual, Efficient phosphate removal from water for controlling eutrophication using novel composite adsorbent, Journal of Cleaner Production 228 (2019) 1311–1319.

[8] R. Nadendla, A. Patchala, A validated high performance liquid chromatographic method for the quantification of favipiravir by PDA detector, International Journal of Life Science and Pharma Research (2021) P181–P188.

[9] T. Azuma, M. Ishida, K. Hisamatsu, A. Yunoki, K. Otomo, M. Kunitou, et al., Fate of new three anti-influenza drugs and one prodrug in the water environment, Chemosphere 169 (2017) 550–557.

[10] S. Sonawane, M.P. Rayaroth, V.K. Landge, K. Fedorov, G. Boczkaj, Thermally activated persulfate-based Advanced Oxidation Processes — recent progress and challenges in mineralization of persistent organic chemicals: a review, Current Opinion in Chemical Engineering 37 (2022), 100839.

[11] G. Boczkaj, A. Fernandes, Wastewater treatment by means of advanced oxidation processes at basic pH conditions: a review, Chemical Engineering Journal 320 (2017) 608–633.

[12] A. Bagheri, A.H. Mahvi, R. Nabizadeh, M.H. Dehghani, B. Mahmoudi, B. Akbari-Adergani, et al., Rapid destruction of the non-steroidal anti-inflammatory drug diclofenac using advanced Nano-Fenton process in aqueous solution, Medica 5 (2017) 879.

[13] K. Kowalska, G. Maniakova, M. Carotenuto, O. Sacco, V. Vaiano, G. Lofrano, et al., Removal of carbamazepine, diclofenac and trimethoprim by solar driven advanced oxidation processes in a compound triangular collector based reactor: a comparison between homogeneous and heterogeneous processes, Chemosphere 238 (2020), 124665.

[14] M.S. Salman, M.C. Sheikh, M.M. Hasan, M.N. Hasan, K.T. Kubra, A.I. Rehan, et al., Chitosan-coated cotton fiber composite for efficient toxic dye encapsulation from aqueous media, Applied Surface Science 622 (2023), 157008.

[15] M.S. Salman, M.N. Hasan, M.M. Hasan, K.T. Kubra, M.C. Sheikh, A.I. Rehan, et al., Improving copper (II) ion detection and adsorption from wastewater by the ligand-functionalized composite adsorbent, Journal of Molecular Structure 1282 (2023), 135259.

[16] M.M. Hasan, K.T. Kubra, M.N. Hasan, M.E. Awual, M.S. Salman, M.C. Sheikh, et al., Sustainable ligand-modified based composite material for the selective and effective cadmium (II) capturing from wastewater, Journal of Molecular Liquids 371 (2023), 121125.

[17] C. Cai, S. Kang, X. Xie, C. Liao, Ultrasound-assisted heterogeneous peroxymonosulfate activation with Co/SBA-15 for the efficient degradation of organic contaminant in water, J Hazard Mater 385 (2020), 121519.

[18] C. Cai, H. Zhang, X. Zhong, L. Hou, Electrochemical enhanced activation of peroxydisulfate by Fe-Co/SBA-15 catalyst for the degradation of Orange II in water, Water research 66 (2014) 473–485.

[19] A. Fernandes, P. Makoś, G. Boczkaj, Treatment of bitumen post oxidative effluents by sulfate radicals based advanced oxidation processes (S-AOPs) under alkaline pH conditions, Journal of Cleaner Production 195 (2018) 374–384.

[20] Z. Wei, F.A. Villamena, L.K. Weavers, Kinetics and mechanism of ultrasonic activation of persulfate: an in situ EPR spin trapping study, Environmental science & technology 51 (6) (2017) 3410–3417.

[21] J. Wen, F. Duan, L. Yang, X. Liu, Y. Huang, G. Ke, et al., The activity and mechanism differences of typical tourmalines in the activation of persulfate for tetracycline degradation, Journal of Solid State Chemistry 314 (2022), 123383.

[22] M. Sabri, A. Habibi-Yangjeh, S. Rahim Pouran, C. Wang, Titania-activated persulfate for environmental remediation: the-state-of-the-art, Catalysis Reviews 65 (1) (2023) 118–173.

[23] Z. Liu, S. Pan, F. Xu, Z. Wang, C. Zhao, X. Xu, et al., Revealing the fundamental role of MoO2 in promoting efficient and stable activation of persulfate by iron carbon based catalysts: efficient Fe2+/Fe3+ cycling to generate reactive species, Water Research 225 (2022), 119142.

[24] J. Li, Y. Liang, P. Jin, B. Zhao, Z. Zhang, X. He, et al., Heterogeneous metal-activated persulfate and electrochemically activated persulfate: a review, Catalysts 12 (9) (2022) 1024.

[25] K.T. Kubra, M.M. Hasan, M.N. Hasan, M.S. Salman, M.A. Khaleque, M.C. Sheikh, et al., The heavy lanthanide of Thulium (III) separation and recovery using specific ligand-based facial composite adsorbent, Colloids and Surfaces A: Physicochemical and Engineering Aspects 667 (2023), 131415.

[26] N. Moradi, M. Jamshidi, R. Ghamarpoor, M.R. Moghbeli, Surface functionalization/silane modification of CeO2 nanoparticles and their influences on photocatalytic activity of acrylic films for methylene blue removal, Progress in Organic Coatings 183 (2023), 107787.

[27] R. Ghamarpoor, A. Fallah, M. Jamshidi, S. Salehfekr, Using waste silver metal in synthesis of Z-scheme Ag@ WO3-CeO2 heterojunction to increase photodegradation and electrochemical performances, Journal of Industrial and Engineering Chemistry 128 (2023) 459–471.

[28] K. Fedorov, M. Plata-Gryl, J.A. Khan, G. Boczkaj, Ultrasound-assisted heterogeneous activation of persulfate and peroxymonosulfate by asphaltenes for the degradation of BTEX in water, J Hazard Mater 397 (2020), 122804.

[29] F. Eftekharipour, M. Jamshidi, R. Ghamarpoor, Fabricating core-shell of silane modified nano ZnO; Effects on photocatalytic degradation of benzene in air using acrylic nanocomposite, Alexandria Engineering Journal 70 (2023) 273–288.

[30] R. Ghamarpoor, A. Fallah, M. Jamshidi, Investigating the use of titanium dioxide (TiO2) nanoparticles on the amount of protection against UV irradiation, Scientific Reports 13 (1) (2023) 9793.

[31] R. Ghamarpoor, M. Jamshidi, A. Fallah, F. Eftekharipour, Preparation of dual-use GPTES@ ZnO photocatalyst from waste warm filter cake and evaluation of its synergic photocatalytic degradation for air-water purification, Journal of environmental management 342 (2023), 118352.

[32] R.D.C. Soltani, Z. Miraftabi, M. Mahmoudi, S. Jorfi, G. Boczkaj, A. Khataee, Stone cutting industry waste-supported zinc oxide nanostructures for ultrasonic assisted decomposition of an anti-inflammatory non-steroidal pharmaceutical compound, Ultrasonics Sonochemistry 58 (2019), 104669.

[33] K. Yaghmaeian, N. Yousefi, A. Bagheri, A.H. Mahvi, R. Nabizadeh, M.H. Dehghani, et al., Combination of Advanced Nano-Fenton Process and Sonication for Destruction of Diclofenac: Variables Optimization Using Response Surface Method, 2022.

[34] C. Cai, Z. Zhang, H. Zhang, Electro-assisted heterogeneous activation of persulfate by Fe/SBA-15 for the degradation of Orange II, Journal of Hazardous Materials 313 (2016) 209–218.

[35] J. Zhou, X. Zhou, K. Yang, Z. Cao, Z. Wang, C. Zhou, et al., Adsorption behavior and mechanism of arsenic on mesoporous silica modified by iron-manganese binary oxide (FeMnOx/SBA-15) from aqueous systems, Journal of Hazardous Materials 384 (2020), 121229.

[36] X. Xu, Y. Yang, Y. Jia, X. Lian, Y. Zhang, F. Feng, et al., Heterogeneous catalytic degradation of 2,4-dinitrotoluene by the combined persulfate and hydrogen peroxide activated by the as-synthesized Fe-Mn binary oxides, Chemical Engineering Journal 374 (2019) 776–786.

[37] J. Liu, Z. Zhao, P. Shao, F. Cui, Activation of peroxymonosulfate with magnetic Fe3O4–MnO2 core–shell nanocomposites for 4-chlorophenol degradation, Chemical Engineering Journal 262 (2015) 854–861.

[38] M. Li, X. Yang, D. Wang, J. Yuan, Enhanced oxidation of erythromycin by persulfate activated iron powder–H2O2 system: role of the surface Fe species and synergistic effect of hydroxyl and sulfate radicals, Chemical Engineering Journal 317 (2017) 103–111.

[39] A.P. Abbott, D. Boothby, G. Capper, D.L. Davies, R.K. Rasheed, Deep eutectic solvents formed between choline chloride and carboxylic acids: versatile alternatives to ionic liquids, Journal of the American Chemical Society 126 (29) (2004) 9142–9147.

[40] X. Ge, C. Gu, X. Wang, J. Tu, Deep eutectic solvents (DESs)-derived advanced functional materials for energy and environmental applications: challenges, opportunities, and future vision, Journal of Materials Chemistry A 5 (18) (2017) 8209–8229.

[41] J. Iqbal, N.S. Shah, M. Sayed, N. Muhammad, S-u Rehman, J.A. Khan, et al., Deep eutectic solvent-mediated synthesis of ceria nanoparticles with the enhanced yield for photocatalytic degradation of flumequine under UV-C, Journal of Water Process Engineering 33 (2020), 101012.

[42] F.M. Perna, P. Vitale, V. Capriati, Deep eutectic solvents and their applications as green solvents, Current Opinion in Green and Sustainable Chemistry 21 (2020) 27–33.

[43] K. Aruchamy, R.N. Maalige, M.M. Halanur, A. Mahto, R. Nagaraj, D. Kalpana, et al., Ultrafast synthesis of exfoliated manganese oxides in deep eutectic solvents for water purification and energy storage, Chemical Engineering Journal 379 (2020), 122327.

[44] S. Sonawane, K. Fedorov, M.P. Rayaroth, G. Boczkaj, Degradation of 1,4-dioxane by sono-activated persulfates for water and wastewater treatment applications, Water Resources and Industry 28 (2022), 100183.

[45] C.G. Burgess, D.H. Everett, S. Nuttall, Adsorption hysteresis in porous materials, Pure and Applied chemistry 61 (11) (1989) 1845–1852.

[46] J.Y. Dong, W.H. Lin, Y.J. Hsu, D.S.H. Wong, S.Y. Lu, Ultrafast formation of ZnO mesocrystals with excellent photocatalytic activities by a facile Tris-assisted antisolvent process, Crystengcomm 13 (20) (2011) 6218–6222.

[47] A. Farhadian, S.A. Kashani, A. Rahimi, E.E. Oguzie, A.A. Javidparvar, S.C. Nwanonenyi, et al., Modified hydroxyethyl cellulose as a highly efficient eco-friendly inhibitor for suppression of mild steel corrosion in a 15% HCl solution at elevated temperatures, Journal of Molecular Liquids 338 (2021), 116607.

[48] H. Wang, A. Zhang, L. Zhang, J. Liu, Y. Han, H. Shu, et al., Study on the influence of compound rust inhibitor on corrosion of steel bars in chloride concrete by electrical parameters, Construction and Building Materials 262 (2020), 120763.

[49] R.D.C. Soltani, M. Mashayekhi, M. Naderi, G. Boczkaj, S. Jorfi, M. Safari, Sonocatalytic degradation of tetracycline antibiotic using zinc oxide nanostructures loaded on nano-cellulose from waste straw as nanosonocatalyst, Ultrasonics Sonochemistry 55 (2019) 117–124.

[50] K. Fedorov, K. Dinesh, X. Sun, R. Darvishi Cheshmeh Soltani, Z. Wang, S. Sonawane, et al., Synergistic effects of hybrid advanced oxidation processes (AOPs) based on hydrodynamic cavitation phenomenon – a review, Chemical Engineering Journal 432 (2022), 134191.

[51] K. Shiraki, T. Daikoku, Favipiravir, an anti-influenza drug against life-threatening RNA virus infections, Pharmacology & therapeutics 209 (2020), 107512.

[52] S.J. Kaptein, S. Jacobs, L. Langendries, L. Seldeslachts, S. Ter Horst, L. Liesenborghs, et al., Favipiravir at high doses has potent antiviral activity in SARS-CoV-2− infected hamsters, whereas hydroxychloroquine lacks activity, Proceedings of the National Academy of Sciences 117 (43) (2020) 26955–26965.